Chapter 2

Reaction diffusion processes on networks

2.1 Introduction

A study included in the thesis relates to Turing instability on regular, random and scale-free networks. The Turing mechanism [4] involves reaction-diffusion (RD) processes which provide the basis for pattern formation in several physical, chemical and biological systems [1-4]. Turing showed [5] that a diffusion-driven instability may occur when infinitesimal perturbations are applied to an initially homogeneous system of reacting and diffusing chemicals. The perturbations may be internally generated due to the fluctuations in the amounts of reactants. The instability gives rise to spatially heterogeneous stationary patterns in the steady state. This is illustrated by considering a system of two chemicals : the activator and the inhibitor. The activator is autocatalytic, i.e., it promotes its own production as well as that of the inhibitor. The inhibitor, as the name implies, inhibits the production of the activator. The diffusion coefficient of the inhibitor is moreover much larger than that of the activator. Consider a homogeneous distribution of the activator and the inhibitor in the RD system. Perturbation is applied to the system through small local increases in the activator concentration. This gives rise to further increases in the concentration of the activator in the local regions due to autocatalysis. The inhibitor concentration is also enhanced locally. The inhibitor, with a higher diffusion coefficient, reaches the surrounding regions first and prevents the activator from spreading into these regions. A nonequilibrium steady state is obtained if the decay of the activator and the inhibitor is offset

by a constant supply of the chemicals. This state is characterised by a stationary distribution of islands of high activator concentration in a sea of high inhibitor concentration. The islands constitute what is known as the Turing pattern.

The Gierer-Meinhardt (GM) model provides a mathematical description of the RD processes, leading to Turing instability, through the partial differential equations

$$\begin{aligned} \frac{\partial a}{\partial t} &= D_a \bigtriangledown^2 a + \rho_a \frac{a^2}{h} - \mu_a a \\ \frac{\partial h}{\partial t} &= D_h \bigtriangledown^2 h + \rho_h a - \mu_h h \end{aligned} \tag{2.1}$$

where 'a' and 'h' are the concentrations of the activator and the inhibitor, D_a, D_h are the respective diffusion coefficients, μ_a, μ_h the removal rates and ρ_a, ρ_h the cross-reaction coefficients. The RD processes described by equation (2.1) are defined in the continuum. In this chapter, we study the formation of Turing patterns in networks with a discrete structure. Three types of network are considered : regular, random and scale-free. The RD processes are described by a simple discretization of equation (2.1). Such discretization, necessary for obtaining numerical solutions of partial differential equations, provides a coupled map model for the networks. Section 2.2 contains a description of the coupled map model the dynamics of which, in specific parameter regions, lead to the formation of Turing patterns in the steady state of the networks. Section 2.3 contains concluding remarks.

Recently, a few studies have been carried out on RD processes occurring on small world networks [14, 15]. Lazaros et al. [14] have studied reactions of the type $A + A \rightarrow 0$ and $A + B \rightarrow 0$ on scale-free networks. The degree distribution of such networks is given by $P(k) \sim k^{-\gamma}$ where the exponent γ is a numerical constant. In the two types of reactions considered, the molecules diffuse on the networks and react when they occupy the same node, two at a time. The RD proesses in scale-free networks are significantly different from those occurring on regular lattices, e.g., the reaction rates are more rapid. Lazaros et al. constructed scale-free networks with different values of γ. For sufficiently large values of γ, the reaction rates are comparable to those for normal lattice models. Again, for sufficiently low values of γ, there is no formation of a depletion zone found on regular lattices (for the reaction $A+A \rightarrow 0$) and no segregation of the reactants (for the $A + B \rightarrow 0$ reactions) in contrast to the behavior observed on regular lattices. Instead what is observed is clusters of A ($A + A$ reaction) and those of A and B ($A + B$ reaction) around the

highly connected nodes of the network. Matthäus [15] has discussed different modeling approaches for the spread of prion disease in the brain. He has investigated the role of Turing-type diffusion driven instability in the formation of plaques which result from local prion accumulations. It has further been shown that RD processes can reproduce the experimental data on prion spread in the mouse visual system. Epidemic models studied on different networks including the scale-free network show that network topology has considerable influence on disease propagation.

2.2 Turing patterns in RD networks

Consider a network of N nodes connected to each other via links. At each node i (i=1,.....,N), the concentration of the activator and the inhibitor are given by a_i and h_i. Time t is discretized in steps of unity and the evolution of the concentration variables is described by the coupled map equations

$$\begin{aligned} a_i(t+1) &= a_i(t) + D_a \textstyle\sum_j C_{ij}(a_j(t) - a_i(t)) + \rho_a \frac{a_i^2(t)}{h_i(t)} - \mu_a a_i(t) \\ h_i(t+1) &= h_i(t) + D_h \textstyle\sum_j C_{ij}(h_j(t) - h_i(t)) + \rho_h a_i^2(t) - \mu_h h_i(t) \end{aligned} \tag{2.2}$$

The coupling matrix C is symmetric with diagonal elements zero and C_{ij} =1 if the nodes i and j are connected and is zero otherwise. The diffusive coupling in equation (2.2) has the form of a finite difference approximation. Under the same approximation, equation (2.1) reduces to equation (2.2) with $\delta t = 1$, $(\delta x)^2 = 1$, where δt is the time increment and δx the mesh size. In the case of networks, however, equation (2.2) defines the coupled map model.

Three different types of networks have been considered : regular, random and scale-free, each with 2500 nodes. The regular network is a square lattice for which the degree of each node, given by the number of links associated with the node, is exactly four. The degree distributions of the random and the scale-free networks are Poissonian and power-law respectively [6,7]. The random network is described by the Erdös-Rényi (ER) model [8]. The network has N nodes and each pair of nodes is connected with probability p_{ER} so that the total number of links in the network is $n = p_{ER} N(N-1)/2$. The scale-free network is generated following the prescription of Barabási et al [9]. One starts with a small number m_0 of nodes. In every time step, a new node with $m \leq m_0$ links is added (m=2 in the present simulation). The new node is connected to an existing node i with probability $\prod(k_i)$ which depends on the

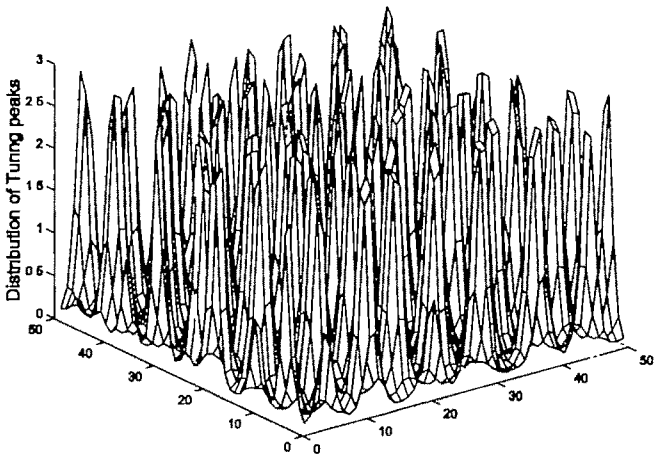

Figure 2.1: Distribution of the Turing peaks in the steady state of a square lattice with 2500 nodes for parameter values $D_a = 0.00055$, $D_h = 0.01$, $\rho_a = \mu_a = 0.00055$ and $\rho_h = \mu_h = 0.0011$.

degree k_i of the node i. The preferential attachment probability is given by

$$\prod(k_i) = \frac{(k_i + 1)}{\sum_j (k_j + 1)} \tag{2.3}$$

After T time steps, the network has $T+m_0$ nodes and $mT + m_0(m_0 - 1)/2$ links assuming all m_0 initial sites to be connected. The evolution rule leads to a scale-free network when the network size is significantly large. The average number of links per node is fixed to be four in both the random and scale-free networks in order that a meaningful comparison with the square lattice results can be made. With $\rho_a = \mu_a$ and $\rho_h = \mu_h$, the steady state ($a_i(t+1) = a_i(t)$, $h_i(t+1) = h_i(t)$) is given by a homogeneous distribution of activator and inhibitor concentration at all the nodes, say, $(a_i, h_i) = (1, 1)$ for all i=1,.....N. This homogeneous steady state is taken to be the initial state of each network. The steady state is perturbed by small amounts ($a_i \rightarrow 1 + \delta a_i$, $h_i \rightarrow 1 + \delta h_i$) at each node using a random number generator. The amount of perturbation is chosen to be the same in the cases of the activator and the inhibitor, i.e., $\delta a_i = \delta h_i$. Time evolution of the perturbed system is determined with the help of equation (2.2). The homogeneous steady state is stable if the perturbed system returns to it after some time steps. The full parameter space corresponding to equation (2.2) contains a region in which the homogeneous steady state is stable. There is another region in the parameter space corresponding to which the perturbed system exhibits Turing instability. The steady state to which the instability leads is obtained if a_i and

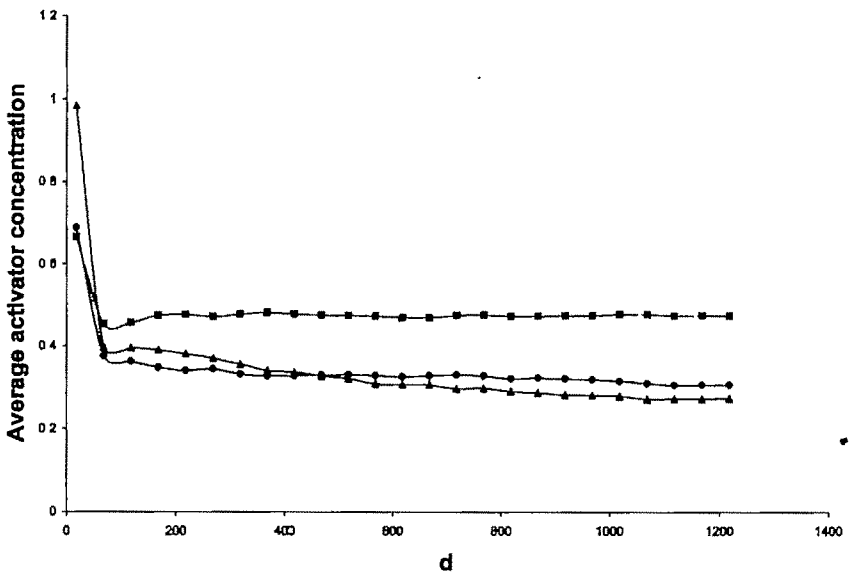

Figure 2.2: Average activator concentration versus $d = D_h/D_a$ in the steady state for $D_h = 0.01$, $\rho_a = \mu_a = 0.00055$ and $\rho_h = \mu_h = 0.0011$. The data points, solid square, solid circle and solid triangle correspond to regular (square-lattice), random and scale-free networks respectively.

h_i change by less than 10^{-4} on five consecutive iterations of equation (2.2) for all i. The state is characterised by a stationary pattern of Turing peaks corresponding to gradients of activator concentration in local regions. The height of a peak is defined as the magnitude of the concentration variable at the highest point of the gradient. Figure 2.1 shows a distribution of Turing peaks in the steady state of a regular network (square lattice with 2500 nodes) with parameter values given by $D_a = 0.00055$, $D_h = 0.01$, $\rho_a = \mu_a = 0.00055$, $\rho_h = \mu_h = 0.0011$.

We now describe the main results of our study on some general aspects of Turing patterns in the steady states of the regular, random and scale-free networks. The initial random number seed is taken to be the same in each case so that the pattern of perturbations at the nodes is identical. Our first observation relates to the fact that the formation of Turing patterns is most favourable, i.e., occurs over a wider region in parameter space in the case of the regular network. Figures 2.2-2.6 are obtained by varying the diffusion coefficient D_a of the activator and keeping the diffusion coefficient D_h of the inhibitor fixed. The variable along the x-axis in each case is the ratio $d = D_h/D_a$. The values of $\mu_a = \rho_a$ and $\mu_h = \rho_h$ are kept fixed at $\mu_a = 0.00055$ and $\mu_h = 0.0011$.

Figure 2.2 shows the average concentration of the activator versus d for the regular, random and scale-free networks. The average is found to be the

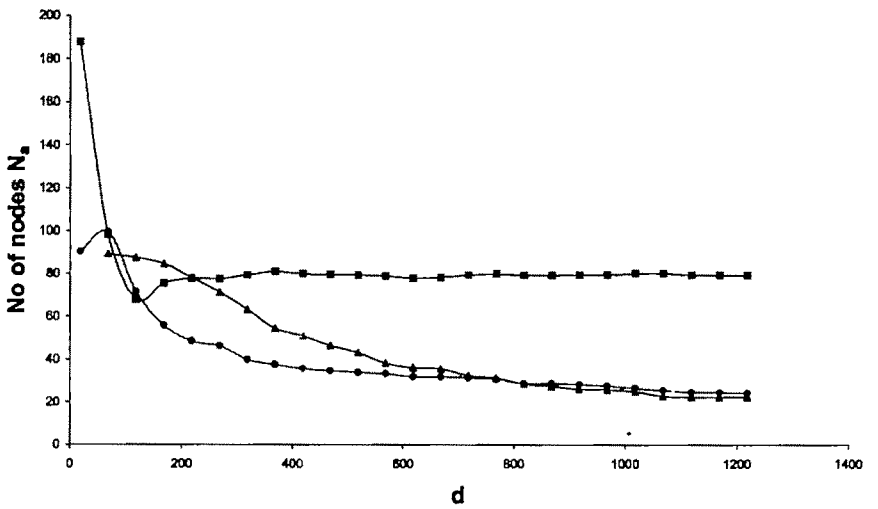

Figure 2.3: Number of nodes N_a at which the activator concentration is greater than equal to a threshold value, versus $d = D_h/D_a$ for $D_h = 0.01$, $\rho_a = \mu_a = 0.00055$, and $\rho_h = \mu_h = 0.0011$. The data points, solid square, solid circle and solid triangle corresponds to regular (square-lattice), random and scale-free networks respectively.

highest in the case of the regular network. Figure 2.3 shows the number of nodes N_a at which the activator concentration a_i is greater than or equal to a threshold value, say 2, versus d. The number of such nodes appears to be the largest in the case of the regular network over almost the full range of d. For smaller values of d, the number of nodes with $a_i \geq 2$ in the case of the scale-free network is greater than the corresponding number for the random network but for larger values of d, the numbers are more or less equal.

Figure 2.4 shows the maximum peak height (equivalently, the highest value of the activator concentration at a node) versus d for the three networks. The maximum height attained in the steady state is more or less the same in the cases of the random and scale-free networks. This value is greater than that in the case of a regular network over the full range of d. Each data point in figures. 2.2-2.4 is an average over five realizations of the steady state. The different realizations are obtained by changing the initial seed of the random number generator. Figure 2.5 shows the connectivity of the node i at which the activator concentration has the highest value in the steady state, versus d. The plot shows an interesting plateau structure. The connectivity is found to shift to higher values for larger d. Figure 2.6 shows the same plot for the scale-free network. The plateau structure is similar to that observed in the case of the random network.

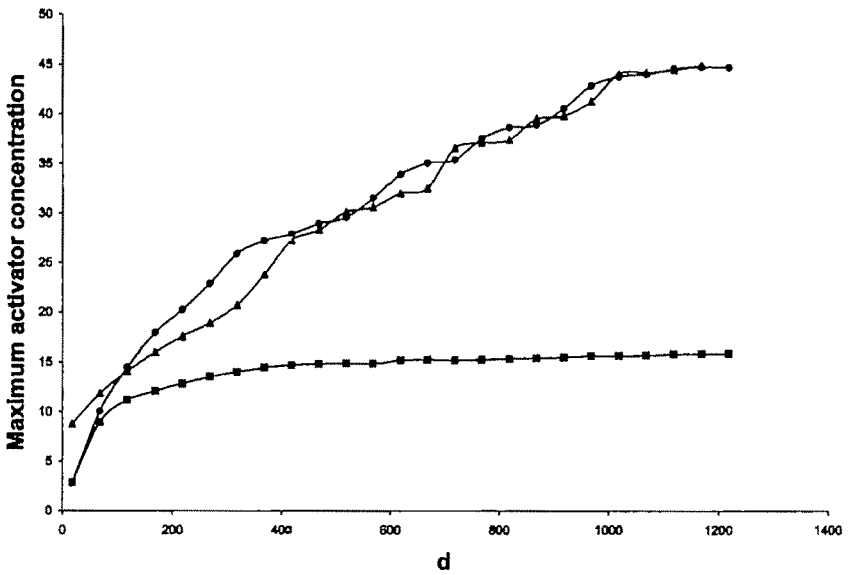

Figure 2.4: Maximum activator concentration versus $d = D_h/D_a$ in the steady state for $D_h = 0.01$, $\rho_a = \mu_a = 0.00055$ and $\rho_h = \mu_h = 0.0011$. The data points, solid square, solid circle and solid triangle corresponds to regular (square-lattice), random and scale-free networks respectively.

From the results obtained, the major conclusion one arrives at is that for the general features of Turing patterns described above, the regular network is markedly different from the random and scale-free networks. The latter two types of networks have more or less similar features. The variation of pattern related quantities as a function of d is smoother in the case of the regular network whereas in the cases of the other two types of networks, the variation is much less smooth. We now look for possible explanations of the results obtained. The important differences between the three networks is that both the random and the scale-free network have a small world (SW) character, i.e., any pair of randomly chosen nodes is connected by a path consisting of a small number of links. This is not true in the case of a regular network like the square lattice. In the first two cases, one can define an average path length L_{av}, which is the average of the shortest paths connecting all pairs of nodes in the network, the length of a path being given by the number of links contained in the path. In the case of the random network, $L_{av} \sim \log N$ where N is the number of nodes in the network. Scale-free networks, with degree exponents in the range $2<\gamma<3$ are ultra -small, i.e., $L_{av} \sim \log\log N$ [10]. In the case of a regular network, L_{av} scales with some power of N, rather than $\log N$. Effective communication between the nodes is thus much greater in the cases of random and scale-free networks. For RD processes, one can define

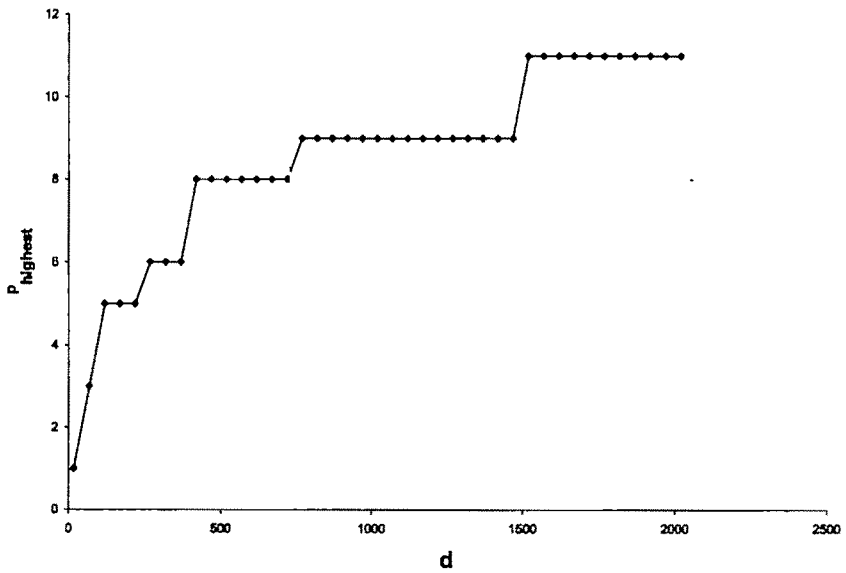

Figure 2.5: $p_{highest}$ versus $d = D_h/D_a$ in the steady state for $D_h = 0.01$, $\rho_a = \mu_a = 0.00055$ and $\rho_h = \mu_h = 0.0011$ in the case of the random network.

two length scales, namely the activator and the inhibitor decay lengths, given by $l_a = \sqrt{(D_a/\mu_a)}$ and $l_h = \sqrt{(D_h/\mu_h)}$ respectively. The decay length provides an estimate of the distance over which molecules diffuse before disappearing due to decay. Turing instability requires short range activation and long range inhibition, i.e., $l_a < l_h$. In obtaining figures 2.2-2.6, the parameters D_h, μ_a, μ_h are kept constant and D_a is varied over the range in which Turing instability occurs. Thus the decay length l_h of the inhibitor is constant with the value $l_h = 3.01$ and the decay length of the activator is decreased from the value $l_a = 1.0$ towards zero. Since the number of nodes in the networks studied is 2500, the average path length L_{av} in the cases of random and scale-free networks is of similar magnitude as l_h. In obtaining the data points in figures 2.2-2.6, the same random number seeds are chosen for each realization (each data point is an average over five realizations), so that the only variation comes from changing the diffusion coefficient D_a of the activator.

Increase in activator concentration at a node is possible if there is a net inflow of activator from the other nodes. Since the largest magnitude of the decay length l_a of the activator is 1.0 (the first data point), increase in activator concentration through diffusion is minimal. Increase in activator concentration at a node occurs mainly through autocatalysis. For this, it is desirable that the amount of activator diffusing away from the node in question is small. Higher concentration of activator is obtained if there is a net outflow

of inhibitor from the node. The steady state concentration of activator at a node is a balance between autocatalysis, inhibition and decay. The average concentration of activator, over the range of $d = D_h/D_a$ studied, is the highest in the case of the regular network. In the cases of random and scale-free networks, the SW feature leads to a greater overall amount of inhibition so that the number of nodes at which the steady state concentration of the activator is above a threshold value (2 in our case) as well as the average concentration of the activator are lower (figures 2.2 and 2.3). The maximum value of the activator concentration in the steady state, when concentrations at all the nodes are considered, is, however, found to be higher than that in the case of a regular network (figure 2.4). The maximum value increases as D_a is lowered . In the case of the regular network, the increase occurs over a small range of values of d and then the maximum concentration value saturates. The increase is steeper and over a much wider range in the cases of random and scale-free networks. In general, there are some nodes at which the activator concentration in the steady state is significantly higher than the maximum value of the concentration in the case of a regular network. However, a larger number of nodes with activator concentration above a threshold value gives rise to a higher average concentration in the case of a regular network. The nodes in the random and scale-free networks have variable connectivity. At some of these nodes, high activator concentration is obtained in the steady state due to autocatalysis being more dominant over inhibition than in the case of a regular network. One example of this is illustrated in figures 2.5 and 2.6. The plots represent connectivity $p_{highest}$ of the node, at which the highest activator concentration occurs, versus $d = D_h/D_a$ with D_h kept constant. The connectivity of a node is the number of links to which the node belongs.The plot exhibits an interesting plateau structure. In this case, the data points are not averaged over five realizations as averaging is expected to destroy the plateau structure. The magnitude of $p_{highest}$ is found to increase on reducing D_a, i.e., increasing $d = D_h/D_a$ (D_h constant). As the same pattern of perturbations is applied for obtaining each data point, the only difference in each case arises from the changed magnitude of D_a. Initially, $p_{highest}$ is low, around 2. A small number of links implies greater isolation and consequent enhancement of autocatalysis which is a local effect. We now discuss the origin of a plateau. As D_a is decreased, the amount of activator remaining at the node and participating in autocatalysis increases. The amount of inhibitor reaching or leaving the node is the same as D_h remains constant. As a

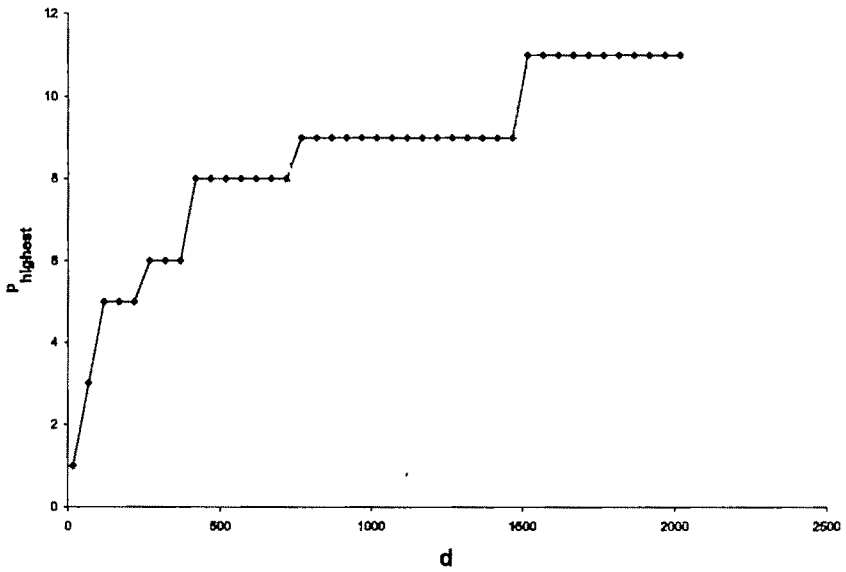

Figure 2.6: $p_{highest}$ versus $d = D_h/D_a$ in the steady state for $D_h = 0.01$, $\rho_a = \mu_a = 0.00055$ and $\rho_h = \mu_h = 0.0011$ in the case of the scale-free network.

result, the highest activator concentration in the steady state increases with lowered values of D_a (figure 2.4). The plateau occurs as long as the node, at which the highest activator concentration is obtained, remains unchanged. The plateau ends when it becomes advantageous for $p_{highest}$ to be raised. Increased number of links may not be detrimental as, because of a lowered value of D_a, the net amount of activator diffusing away is still small whereas an increased number of links allows a greater amount of inhibitor to leave the node, leading to higher activator concentration in the steady state. The plateau structure is seen for other sets of parameter values also. Figure 2.7 shows the distribution of activator concentration in the steady states of the regular and scale-free networks for $D_a = 0.000015$ and $D_h = 0.01$. The bin size is taken to be 0.5. An average over ten realizations has been taken. The data for the random network are not plotted for clarity. The distribution in this case is similar to that of the scale-free network.

2.3 Summary and Discussion

In this Chapter, we have studied the formation of Turing patterns in the cases of regular, random and scale-free networks. The RD processes are described by a model which is a simple discretized version of the GM model. Formation of Turing patterns is most favourable in the case of the regular network

(square lattice). The size of the network is kept the same in each case. The average degree of nodes is four in the cases of the random and scale-free networks so that a meaningful comparison with square lattice results can be made. Some general features of Turing patterns in the steady state have been studied like the average activator concentration versus $d = D_h/D_a$, the ratio of the diffusion coefficients of the inhibitor and the activator, the number of nodes N_a at which the activator concentration a_i is greater than or equal to a threshold value versus d, the highest value of a_i versus d, and the distribution of activator concentration amongst the network sites. In each case, the results for the random and the scale-free networks are markedly different from those of the regular network. The differences can be explained in terms of the small world character of the first two types of networks, These networks also exhibit an interesting plateau structure in a plot of the connectivity of the node t at which the activator concentration has the highest value in the steady state, versus d. Figure 2.7 provides clear evidence that the distribution of the activator concentration amongst the nodes of the network is markedly different in the cases of regular and random/scale-free networks. The scale-free network, considered in the thesis, is of the Barabási - type with the degree exponent $\gamma \sim 3$. For this high value of γ, the number of highly connected nodes is very small which may be the reason why the scale-free and random networks exhibit similar features. The value of D_h, the diffusion coefficient of the inhibitor has been kept constant to identify the systematic trends associated with the variation of D_a. The range of D_h values for which Turing patterns form in the steady state is not sufficiently long to study the variation with respect to D_h, keeping D_a fixed. We have, however, verified that the results reported in the thesis hold true for other values of D_h as well as for different parameter sets.

RD processes are associated with many chemical and biological systems [1-4]. In neurobiology, there is considerable evidence that synaptic transmission may not be the exclusive mechanism for neurotransmission in brain functions. There are suggestions [11] that nonsynaptic diffusion neurotransmission plays a fundamental role in certain sustained brain functions which include vigilance, hunger, mood, responses to certain sensory stimuli as well as abnormal functions like mood disorder, spinal shock, spasticity and drug addiction. Liang [11] has proposed a RD neural network model to demonstrate the advantages of nonsynaptic diffusion from a computational viewpoint. The RD processes considered are described by the GM model. The spa-

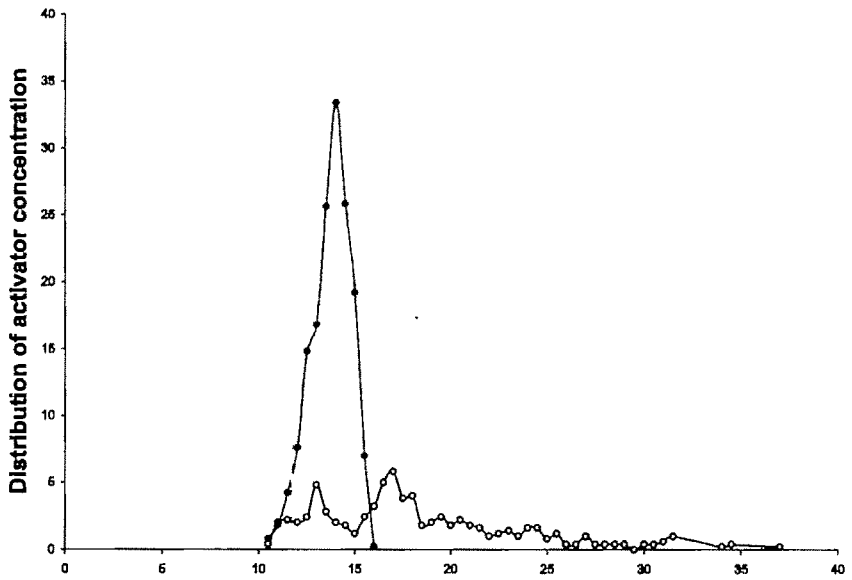

Figure 2.7: Distribution of activator concentration amongst the network sites in the steady states of the regular (solid dots) and scale-free (open circles) networks.

tial Laplacian operator is approximated by finite differences since in a neural network, the neurons are located at discrete positions. The activator and the inhibitor of the GM model are produced by the neurons of the network. Due to Turing-type instabilities, the network can support multiple simultaneous spatiotemporal organization processes. In fact, the Turing islands of activator concentration gradients may correspond to distinct areas of brain activity. Liang considered the RD processes on a square network but a real neural network is more like a random graph with a SW character [6,7]. The present study clearly shows that the Turing patterns on random scale-free networks have characteristics distinct from those in the case of a regular network. The existence of higher concentration gradients in the first two cases may imply sharper signaling response whereas lower numbers of Turing peaks possibly favour the emergence of nonoverlapping, i.e., distinct functional areas. Biological networks like gene transcription regulatory and metabolic reaction networks have a scale-free character [6,7,12]. These networks serve as scaffolds for various RD processes. There has been suggestions that specific biological activities may be controlled by concentration gradients of appropriate type arising out of Turing-like instabilities [1]. In general, RD processes may give rise to other types of instabilities leading to stationary, oscillatory and travelling wave patterns. It will be of considerable interest to find specific examples of patterns generated by RD processes in biological networks. A

deeper question relates to the small world character of such networks and its role in essential biological phenomena.

Bibliography

[1] Koch A J and Meinhardt H 1994 Biological pattern formation: from basic mechanisms to complex structures Rev. Mod. Phys. **66** 1481-1507

[2] Murray J D 1993 Mathematical Biology, Springer-Verlag, Berlin, Heidelberg New York

[3] Maini P K, Painter K J and Chau H N P 1997 Spatial pattern formation in chemical and biological systems J. Chem. Soc., Faraday Trans. **93** 3601-3610

[4] A. De Wit 1999 Spatial patterns and spatiotemporal dynamics in chemical systems Adv. Chem. Phys. **109** 435-513

[5] Turing A M 1952 The chemical basis of morphogenesis Phil. Trans. R. Soc. London B **237** 37-72

[6] Albert R and Barabási A -L 2002 Statistical mechanics of complex networks Rev. Mod. Phys. **74** 47-97

[7] Newman M E J 2003 The structure and function of complex networks SIAM Review **45** 167-256; cond-mat/0303516

[8] Erdös P and Rényi A 1960 The Evolution of Random Graphs Publications of the Mathematical Institute of the Hangarian Academy of Sciences **5** 17-61

[9] Barabási A -L, Albert R and Jeong H 1999 Mean-field theory for scale-free random networks Physica A **272** 173-187

[10] Barabási A -L and Oltvai Z N 2004 Network biology: understanding the cell's functional organization Nature Reviews Genetics **5** 101-113

[11] Liang P 1995 Neurocomputation by reaction diffusion Phys. Rev. Lett. **75** 1863-1866

[12] Alm E and Arkin A P 2003 Biological Networks Current Opinion in Structural Biology **13** 193-202

[13] Bose I 2002 Biological Networks cond-mat/0202192

[14] Lazaros K G and panos Argyrakis 2004 Absence of kinetic effects in reaction-Diffusion Processes in scale-free networks, Physical Review Letter 92 13

[15] Matthäus F 2006 Diffusion versus network models as description for the spread of prion diseases in the brain, Journal of Theoretical Biology, 240 104-113.